

TDMA Scheduling in Spatially Extended LiFi Networks

JONA BEYSENS¹ (Member, IEEE), JEAN-PAUL M. G. LINNARTZ^{2,3} (Fellow, IEEE),
DRIES VAN WAGENINGEN³, AND SOFIE POLLIN¹ (Member, IEEE)

¹Department of Electrical Engineering, KU Leuven, 3000 Leuven, Belgium

²Department of Electrical Engineering, Eindhoven University of Technology, 5600 Eindhoven, The Netherlands

³Department of IoT Infrastructure, Research, Signify (Philips Lighting), 5656 Eindhoven, The Netherlands

CORRESPONDING AUTHOR: J. BEYSENS (e-mail: jona.beysens@kuleuven.be)

The work of Jona Beysens was supported in part by the Research Foundation Flanders (FWO) SB Doctoral Fellowship under Grant 1S59918N.

ABSTRACT Optical Wireless Communication (OWC) has attracted significant attention from academia and industry as a promising solution to complement traditional radio frequency communication. In Light-Fidelity (LiFi) networks, to enable soft handover and provide robustness against blockage of the line-of-sight links, LiFi receivers are designed to see multiple LiFi transmitters within their field-of-view. To trade-off spatial multiplexing with harmful interference, a proper user scheduling technique is required. In this work, we first derive practical and exact expressions for determining which simultaneous transmissions will create harmful interference and should be scheduled in multiple time-slots. Afterwards, relying on this expression, we propose our semi-distributed *Spatially Extended TDMA* algorithm, which is based on a time division contention-free access scheme. In contrast to more complex algorithms in the state-of-the-art, our scheduling protocol can reduce the computation time while also achieving a superior minimal user throughput. For a scenario with 9 transmitters and up to 15 receivers, our protocol is at least a factor 120 faster and can improve the minimal user throughput up to 91%, making it suitable for practical roll-out as a promising solution for very dense LiFi networks.

INDEX TERMS Access protocols, optical wireless communication, scheduling algorithms, time division multiple access.

I. INTRODUCTION

OPTICAL Wireless Communication (OWC) is a promising solution to offer ultra-reliable communication in ultra-dense scenarios. As a result, it has attracted significant attention from academia and industry to complement traditional radio frequency (RF) communications. In a Light-Fidelity (LiFi) network, light-emitting diodes (LEDs) are employed as transmitters (TXs), while users can receive the emitted light signal with a receiver (RX) such as a photo diode or a camera. These LED transmitters have a local and narrow, but nonetheless overlapping coverage region, and as a result, LiFi networks can potentially serve a large number of users with a large number of non-interfering transmitters, all using the same spectrum while creating narrow signal regions around the intended receiver. For handover and robustness against blockage of the line-of-sight (LOS), RXs

are designed to see multiple TXs within their field-of-view (FOV). This inevitably results in strong contention and inter-user interference. Nonetheless, guaranteed quality of service (QoS), free of random back-offs after message collision, is one of the main drivers for the adaptation of LiFi in the market today. This is also reflected in the latest standardization for LiFi networks. A new medium access control (MAC) protocol is proposed in the IEEE P802.15.13 task group which controls medium access in a deterministic manner to guarantee the QoS [1]. In literature, several centralized and scheduling-based approaches have been investigated that rely on sufficient knowledge about the network topology, but it is well known that schedule-based and centrally controlled schemes do not scale to very large networks.

Frequency division multiple access (FDMA) is commonly used in LiFi research. A fractional frequency reuse scheme to

avoid interference for cell-edge users is considered in [2], [3]. However, this requires accurate frequency synchronization among TXs. Further, this frequency allocation is fixed, thus it is not able to adapt to variations in user distribution. In [4]–[6], an OFDMA scheme is used to mitigate intra-cell interference, but since inter-cell interference is not addressed, the performance deteriorates in dense user networks.

Time Division Multiple Access (TDMA) is an alternative scheduling method to avoid interference by allocating non-overlapping time-slots to different users. In [7], [8], a Single-Input-Single-Output (SISO) architecture is considered, in which every RX is served by a single TX. Time fractions of users are optimized to maximize the proportional fairness. However, two users close to each other associated to different TXs can unfortunately still be served simultaneously, as there is no fine-grained interference control. In [9], the spectral efficiency is maximized by properly selecting the time fractions and allocated power for each user. However, the network is limited to a single TX without considering interference from other nearby TXs.

Also user-centric algorithms are investigated, in which users first are clustered in groups and then TXs are associated to these user groups. In [10], a graph based approach is used to cluster users in groups and based on this a fine-grained scheduling algorithm is proposed handling which RX should be served by which TX in every time-slot. In [11], a MIMO architecture with vectored transmission and zero-forcing precoding is employed in every user group. However, [12] shows that closely spaced users can result in an ill-conditioned channel matrix, degrading the performance of zero-forcing precoding. Their solution is to consider user groups of different sizes and assign time fractions to these groups to maximize the proportional fairness. So when the channel correlation is high, small size user groups will be assigned large proportions of time-slots to mitigate the negative effect of high channel correlation.

In addition to scheduled approaches, distributed contention schemes exist that rely on carrier sensing to decide whether channel access is allowed. In [13], the amount of discarded packets due to channel access failures is reduced by dynamically adjusting the Clear Channel Assessment (CCA) thresholds. Carrier Sensing can avoid harmful interference, but in OWC ceiling-based TXs do not necessarily see each other to coordinate downlink transmissions, while these must convey a busy tone to signal incoming uplink signals. Although these approaches scale well, they require dedicated control signals in OWC, while in this article we show that such mutual exchange of control can be used better. An ideal protocol is centrally controlled, while distributing as much as possible decisions for scalability. An ideal protocol, can approximate with high accuracy what nodes can transmit at the same time efficiently. Moreover, QoS, fairness, and assessments for how many users can be accepted with a guaranteed minimum throughput and latency, can all be better handled if the system does not have to rely on competition and randomized collision resolution.

In this work, we propose a mathematical framework to decide when two parallel transmissions are allowed and when they should be prohibited by setting up TX coordination [14]–[16]. This framework is then exploited by a central controller to come up with a set of time-channels including a feasible scheduling scheme for the TXs, determining which RXs can be served in these time-channels. Based on this scheme, the TXs distributively schedule their RXs in time. The goal is to provide a low-complexity scheduling scheme. We focus on dense user networks, in which the number of RXs is larger than the number of TXs. The main contributions of this work are summarized as follows:

- We derive the mathematical criteria to decide when two neighbouring parallel transmissions are harmful and should be prohibited by setting up TX coordination. Extensive analysis is performed and geometric interpretations are derived. The criteria are verified with the scenario in which the aggregate interference from all neighbouring TXs is considered instead of only one. Yet, the proposed criteria are simpler and require little processing power (Section III).
- We propose a two-level scheduling algorithm, named Spatially Extended TDMA (SE-TDMA), in which the coarse-grained time-channel allocation is performed in a central controller and the fine-grained time-slot scheduling is distributively performed on every TX. By splitting and distributing the scheduling task, the workload of the central controller is reduced and the system is less vulnerable to a single point of failure. Further, the communication overhead with the central controller is minimized (Section IV).
- We evaluate the performance of SE-TDMA by extensive simulations. Further, we compare SE-TDMA with two related state-of-the-art research works. We show that we can get superior performance in networks with a low user density and that we reach the only practically feasible solution in dense user networks due to the high complexity of the state-of-the-art algorithms (Section V).

II. SYSTEM MODEL

We consider a LiFi network with N_t transmitters (TX) and N_r receivers (RX). The set of all transmitters and receivers is denoted as \mathcal{N}_t and \mathcal{N}_r , respectively. The TXs are mounted on the ceiling in a rectangular grid with inter-TX distance Δ_t and are equipped with an infrared LED for downlink transmission and a photo diode sensitive to infrared light for uplink reception. Similarly, the RXs contain a photo diode for downlink reception and an LED for uplink transmission. In this way, the LiFi system supports bidirectional communication. We assume that the time is divided in discrete time-slots, and that every RX communicates with a single TX at a time and vice versa, i.e., we consider a Single-Input-Single-Output (SISO) architecture. The TXs periodically send pilot signals, from which the RXs acquire the channel state information (CSI) and transfer it to the

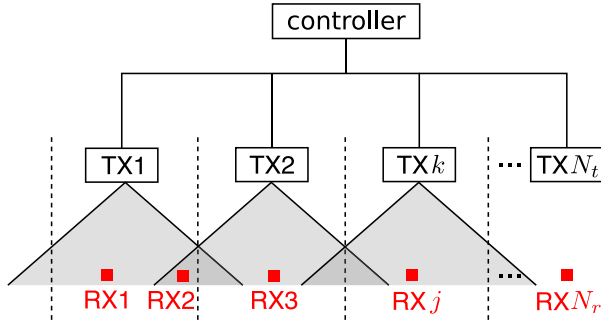


FIGURE 1. System architecture. The gray region represents the coverage region of a TX, which is defined in Section II-B.

central controller via the uplink return channel. We assume that the channel is measured frequently enough such that the impact of outdated channel information (due to user mobility) on the performance is negligible. Further, we consider a reliable return channel and thus the CSI can be retrieved by the central controller without transmission errors. The return channel only carries small amounts of data and for our purpose we only occasionally need to add some extra payload. Therefore, it is reasonable to assume that the return channel is not the limiting factor and that considering it in our system performance evaluation does not add relevant insights but only obscures the discussion of the dominant effects in the downlink. Lastly, in the evaluations, we assume that the line-of-sight path is always available. That is, the effect of blockage due to humans, equipment or furniture is not quantified, although some of the protocols can handle this. The system architecture is presented in Fig. 1. The index k is used to represent a transmitter, whereas the index j is used to represent a receiver.

We first present the LiFi channel model. Afterwards, we define the relevant regions which will be used in the derivation of the mathematical criteria in Section III.

A. LIFI CHANNEL MODEL

Since optical wireless communication is strongly line-of-sight (LOS) dominated, it is sufficient to solely consider the LOS signal propagation. We model the channel matrix $\mathbf{H} = [h_{k,j}] \in \mathbb{R}^{N_t \times N_r}$ as:

$$h_{k,j} = \begin{cases} \frac{(m+1)A_{pd}}{2\pi d_{k,j}^2} \cos^m(\phi_{k,j}) g(\psi_{k,j}) \cos(\psi_{k,j}), & |\psi_{k,j}| \leq \Psi_c \\ 0, & \text{otherwise} \end{cases} \quad (1)$$

where $m = \frac{-\ln(2)}{\ln(\cos \phi_{1/2})}$ is the Lambertian order of the LED in with $\phi_{1/2}$ the half power semi-angle, A_{pd} the collection area of the photo diode, $d_{k,j}$ the distance between TX k and RX j , $\phi_{k,j}$ and $\psi_{k,j}$ the irradiation angle and incidence angle, respectively, $g(\psi_{k,j})$ the concentrator and filter gain of the photo diode, and Ψ_c the field-of-view of the receiver. The signal-to-interference-plus-noise-ratio (SINR) at RX j in

time-slot s is computed as follows¹:

$$\text{SINR}_{s,j} = \frac{\sum_{k=1}^{N_t} f_{k,j,s} (\alpha h_{k,j})^2}{N + \sum_{j'=1}^{N_r} \sum_{k'=1, k' \neq j}^{N_t} f_{k',j',s} (\alpha h_{k',j'})^2}, \quad (2)$$

with N the noise power and $\mathbf{F} = [f_{k,j,s}] \in \{0, 1\}^{N_t \times N_r \times N_s}$ the time-slot scheduling tensor, in which $f_{k,j,s}$ indicates whether RX j is served by TX k in time-slot s and N_s denotes the number of time-slots. The parameter $\alpha = \rho \eta P_c$, with ρ the responsivity of the photo diode, η the wall-plug efficiency of the LED (i.e., the energy conversion efficiency from electrical to optical power) and P_c the electrical transmission power for communication. Since in every time-slot, a TX can serve at most one RX and one RX can served by only one TX, $\max_k \sum_j f_{k,j,s} = 1 \forall s$.

We do not consider a frequency-dependent response of the LEDs. This can for instance be reached by applying a pre-emphasis circuit at the transmitters, in which higher frequencies are boosted such that the output spectrum of the LED channel is assumed to be flat across the frequency range $[0, B]$, with B the communication bandwidth. The achievable throughput at RX j in time-slot s can be modelled as [17]:

$$R_{s,j} = B \log_2 \left(\frac{1}{\Gamma} \text{SINR}_{s,j} + 1 \right), \quad (3)$$

in which Γ denotes an implementation gap to reflect the performance in real-life scenarios ($\Gamma \geq 1$).

B. DEFINITIONS OF REGIONS

Following the channel model, signal quality will degrade as function of the distance between the transmitter and receiver. In addition, neighboring transmitters will create harmful interference with a given interference strength. We now define multiple relevant regions. The challenge is then to find adequate expressions using measured metrics, which are used in the scheduling protocol. The expressions considered in this work are exclusively based on the received signal strength and do not depend on the position of the receivers. An illustration of the defined regions is presented in Fig. 2.

1) COVERAGE REGION

We focus on the downlink transmissions and we define the **coverage region** of a TX k as the region in which the Signal-To-Noise ratio (SNR) to a RX j is sufficient such that RX j can decode transmitted information from that TX k . The coverage region is illustrated in Fig. 1. RX j can be associated to TX k or to another TX, as defined next.

2) ASSOCIATION REGION

In the protocol, RX j is associated to the TX k with the highest signal strength. Therefore, we define the **association region**

1. Throughout this work, index k is used to denote the desired TX, whereas index k' is used to represent an interfering TX k' with respect to TX k .

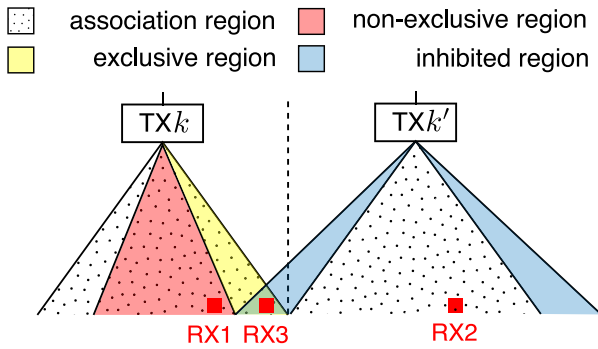


FIGURE 2. Illustration of definitions of regions.

of a TXk, represented by $\mathcal{A}_k = \{j \in \mathcal{N}_r \mid k = \arg \max_k h_{k,j}\}$, as the region in which the protocol associates present RXs to that TXk. This region is a subset of the coverage region and is illustrated with dots in Fig. 2. The dashed line denotes the middle position between TXk and TXk'. In this example, RX1 and RX3 are associated to TXk and RX2 is associated to TXk'. For line-of-sight propagation conditions from typical Lambertian emitters and a square grid of TXs, which is typically used in indoor lighting based installations, the association region is also a square, the side length of which equals the inter-TX distance Δ_T . In more general deployments, the association region can be represented by a Voronoi polygon, which consists of all RX locations closer to that TX than to any other, as the channel strength is inversely proportional to the distance.

3) EXCLUSIVE REGION

For handover and robustness against blockage of the LOS signal, RXs are designed to see multiple TXs within their field-of-view. Therefore, RXs are subject to interference from nearby TXs. To quantify this, we define an **exclusive region** of a TX as a subset of the association region where the protocol decides that users are subject to excessively harmful interference from neighboring cells, and claims exclusive use, i.e., prohibits simultaneous transmissions by other TX that are too close. We call users in this region exclusive users. For these exclusive users, the scheduling protocol should ensure exclusive channel access, which can be realised by silencing neighboring TXs.

In particular, the exclusive region of TXk with respect to TXk', represented by $\mathcal{E}_{kk'}$, is defined as the region inside the association region of TXk where users should get exclusive access to the channel and transmissions from TXk' should be silenced. Ideally, the exclusive region can be determined locally by the TX, so the TX knows for which transmissions exclusive slots should be negotiated.

4) NON-EXCLUSIVE REGION

The **non – exclusive region** of TXk, represented by $\bar{\mathcal{E}}_k$, is then defined as the region in which the protocol decides that users are *not harmed* by the neighboring cell interference. We call users in this region non-exclusive users. For this region, the TX does not need to negotiate exclusive slots.

The non-exclusive region of TXk and the exclusive regions of TXk with respect to all neighbouring TXk' are disjoint sets and the union of those make up the association region of TXk, i.e.,

$$\left(\bigcup_{k'} \mathcal{E}_{kk'} \right) \cap \bar{\mathcal{E}}_k = \emptyset \quad (4)$$

$$\left(\bigcup_{k'} \mathcal{E}_{kk'} \right) \cup \bar{\mathcal{E}}_k = \mathcal{A}_k. \quad (5)$$

In the illustration in Fig. 2, RX3 is located in the exclusive region of TXk due to the presence of neighbouring TXk', and therefore TXk' cannot be active when RX3 is being served by TXk. Therefore, two orthogonal channels are required for this distribution of RXs. In this work, we make the channels orthogonal in time: TXk gets time-channel 1 and TXk' gets time-channel 2. Further, since RX1 is located in the non-exclusive region of TXk, TXk allows TXk' to transmit in parallel to one of its non-exclusive RXs (e.g., RX2) when TXk is serving RX1.

5) INHIBITED REGION

From the perspective of the interfering TXk', the union of exclusive regions of neighbouring cells k make up the region in which TXk' is inhibited to transmit, which we define as the **inhibited region** of TXk', denoted as $\mathcal{I}_{k'} = \bigcup_k \mathcal{E}_{kk'}$. So if there is an RX located in the inhibited region of TXk', then the protocol determines that TXk' is *inhibited* to transmit when that RX is scheduled. In any practical system, the size of the inhibited region of a TX extends beyond its association region.

The key challenge is to find an expression for this inhibited region, both ideally and practically. When is interference harmful? When it exceeds a threshold, or only when it impacts the link capacity beyond a threshold? And how can TXk and TXk' in a practical system determine unambiguously which users are in the exclusive region of TXk and hence in the inhibited region of TXk'?

C. SCHEDULING WITH INHIBITED REGION

We illustrate in Fig. 3 how the Spatially Extended TDMA scheduling protocol exploits knowledge of the inhibited region, where TX1 and TX2 have unambiguously defined their non-exclusive and inhibited regions. In general, the protocol works as follows. First, the downlink channel qualities are measured and transferred to the central controller via the uplink channel. Based on this, the controller associates every RX to a TX and makes an overview of which RX is located in which inhibited region. Since in this example, RX1 is located in the inhibited region of TX2, TX2 should be silent when TX1 is transmitting to RX1, as TX2 would generate harmful interference to RX1. Therefore, the protocol decides to use two non-overlapping time-channels for this distribution of RXs, in which the green and blue time-channel is allocated to TX1 and TX2, respectively. We indeed observe

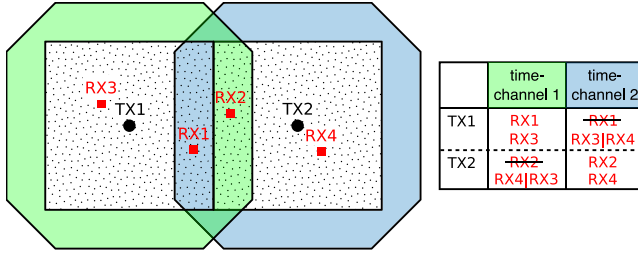


FIGURE 3. Implication of inhibited region on time scheduling (considering the rate-based inhibited region derived in Section III-B). The association region is denoted by the dotted area. The table summarizes the transmission possibilities of TXs to serve their associated RXs, in which RX3|RX4 means that RX3 is not crossed out if TX2 serves RX4.

from the table in Fig. 3 that TX2 cannot be active when TX1 serves RX1. However, TXs can opportunistically use a free time-channel if there is no conflict with its neighbours. In the example, TX1 can serve RX3 in the blue time-channel, but only when TX2 is serving RX4, as RX4 is not harmed by TX1.

III. DERIVATION OF INHIBITED REGION

In this section, we will formalize the criteria for two different choices of the inhibited region, which will be used in the scheduling protocol presented in Section IV. The first definition defines harmful interference as a fixed interference level, while the second definition defines harmful interference as the interference that would result in a 50% data rate degradation. In a spatial representation, the first definition draws a circle around an interfering transmitter, while the second definition draws a series of lines at a given distance between the interfering and serving transmitters.

A. SIGNAL-BASED INHIBITED REGION

A simple choice for the inhibited region of TXk' is the region in which the signal strength of TXk' exceeds a particular threshold. We refer to this region as the signal-based inhibited region of TXk' , denoted as $\mathcal{I}_{k'}^s$. The signal-based inhibited region can be characterized as follows.

Definition 1: Assume RXj is in the association region of TXk , i.e., $j \in \mathcal{A}_k$. Then, RXj is located in the signal-based inhibited region of TXk' if and only if:

$$RXj \in \mathcal{I}_{k'}^s \Leftrightarrow \frac{\alpha^2 h_{k',j}^2}{N} \geq \chi, \quad (6)$$

with χ the harmful interference threshold power level.

For a radially symmetric TX emission pattern, the signal based inhibited region has a circular shape in a spatial representation and the value of χ is inversely proportional to the size of the inhibited region. Although the signal-based inhibited region only depends on the signal of the interfering TXk' , which is represented by $h_{k',j}$ in (6), the challenge is to determine a good value for the parameter χ . A discussion on the selection of this parameter χ and a visualization of the circular signal-based inhibited region will be presented in Section III-D.

B. RATE-BASED INHIBITED REGION

In this section, we extend the definition of the inhibited region of TXk' to not only consider the signal strength of TXk' , but also considering the signal strength of neighbouring TXk . In particular, we find an elegant expression that optimizes the data rate of the user which experiences interference from TXk' . Therefore, we will refer to this region as the rate-based inhibited region.

Similarly as before, we denote the rate-based inhibited region of TXk' as $\mathcal{I}_{k'}^r$. We derive an expression for this region in two steps. First, we derive an expression of the rate-based exclusive region of TXk with respect to TXk' , denoted as $\mathcal{E}_{kk'}^r$. Then, the rate-based inhibited region is found as the union of the exclusive regions, i.e., $\mathcal{I}_{k'}^r = \bigcup_k \mathcal{E}_{kk'}^r$.

We consider a setup consisting of two neighbouring transmitters TXk and TXk' and a receiver RXj which is located in the association region of TXk , i.e., $RXj \in \mathcal{A}_k$. Thus, TXk acts as the serving TX and TXk' acts as the interfering TX. To find the exclusive region of TXk with respect to TXk' , we consider two scheduling strategy cases: a) TXk serves RXj for 50% of the time, *without interference* from TXk' and b) TXk serves RXj for 100% of the time, *with interference* from TXk' . The throughput in these cases is denoted by R_a (without interference) and R_b (with interference), respectively. Assuming the SNR is large ($\alpha^2 h_{k,j}^2 \gg N$) in the association region and the system is interference limited ($\alpha^2 h_{k',j}^2 \gg N$), then R_a is given by:

$$R_a = \frac{1}{2} B \log_2 \left(\frac{\alpha^2 h_{k,j}^2}{\Gamma N} + 1 \right) \quad (7)$$

$$\approx \frac{1}{2} B \log_2 \left(\frac{\alpha^2 h_{k,j}^2}{\Gamma N} \right). \quad (8)$$

Similarly, R_b can be written as:

$$R_b = B \log_2 \left(\frac{\alpha^2 h_{k,j}^2}{\Gamma (N + \alpha^2 h_{k',j}^2)} + 1 \right) \quad (9)$$

$$\approx B \log_2 \left(\frac{\alpha^2 h_{k,j}^2}{\Gamma \alpha^2 h_{k',j}^2} \right), \quad (10)$$

so the difference can be described by:

$$R_b - R_a = B \left[\log_2(\alpha^2 h_{k,j}^2) - \log_2(\Gamma \alpha^2 h_{k',j}^2) - \frac{1}{2} \left(\log_2(\alpha^2 h_{k,j}^2) - \log_2(\Gamma N) \right) \right]. \quad (11)$$

This means that one can derive a rule of thumb identifying if parallel transmission gives favorable total throughput, namely:

$$R_b > R_a \Leftrightarrow \frac{\alpha^2 h_{k,j}^2}{\Gamma \alpha^2 h_{k',j}^2} \sqrt{\frac{\Gamma N}{\alpha^2 h_{k,j}^2}} > 1 \quad (12)$$

$$\Leftrightarrow \frac{\alpha^2 h_{k,j}^2}{(\alpha^2 h_{k',j}^2)^2} \frac{N}{\Gamma} > 1. \quad (13)$$

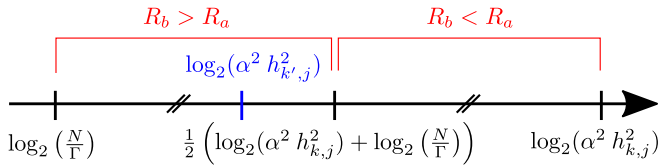


FIGURE 4. Illustration of expression for exclusive region $\mathcal{E}_{kk'}^r$.

Looking more closely to the cross-over point between R_b and R_a , gives us the following insight:

$$R_b = R_a \Leftrightarrow \log_2(\alpha^2 h_{k,j}^2) - \log_2(\Gamma \alpha^2 h_{k',j}^2) = \frac{1}{2} \left(\log_2(\alpha^2 h_{k,j}^2) - \log_2(\Gamma N) \right) \quad (14)$$

$$\Leftrightarrow \log_2(\alpha^2 h_{k',j}^2) = \frac{1}{2} \left(\log_2(\alpha^2 h_{k,j}^2) + \log_2\left(\frac{N}{\Gamma}\right) \right). \quad (15)$$

The cross-over point is, on a log scale, located where the interference term is exactly in the middle of the signal term and the noise term. As capacity expressions also take a logarithm of signal-to-noise ratios, this implies that half the ideal interference-free capacity can be achieved. The same rate can be obtained when time-sharing with two TXs. If the interference term is smaller than this midpoint, then it is better to allow interference. If the interference term is larger than this middle point, then it is better to avoid interference. A visualization is presented in Fig. 4. This leads to the following definition.

Definition 2: Assume RXj is in the association region of TXk, i.e., $j \in \mathcal{A}_k$. Then, RXj is located in the rate-based exclusive region of TXk with respect TXk' if and only if:

$$RXj \in \mathcal{E}_{kk'}^r \Leftrightarrow \frac{\alpha^2 h_{k,j}^2}{(\alpha^2 h_{k',j}^2)^2} \frac{N}{\Gamma} < 1. \quad (16)$$

Further, if RXj is in the rate-based exclusive region of TXk with respect to TXk', then by definition, RXj belongs to the rate-based inhibited region of TXk':

$$RXj \in \mathcal{E}_{kk'}^r \Rightarrow RXj \in \mathcal{I}_{k'}^r. \quad (17)$$

C. INSIGHTS IN THE RATE-BASED INHIBITED REGION

Interestingly, (16) only requires channel state information and does *not* need RX location information. Somewhat counter intuitively, we observe that even for an interference-limited system $\alpha^2 h_{k',j}^2 \gg N$, the optimal strategy for allowing or prohibiting simultaneous transmission highly depends on the system noise floor. In the extreme noise-free case, $N \rightarrow 0$, $h > 0$, parallel transmission should always be prohibited.

Based on (16), we can prove that in any practical system in which the SNR in the association region is large, the size of the rate-based inhibited region in a spatial representation extends beyond its association region. Let us assume α is constant, i.e., all TXs use the same transmission power.

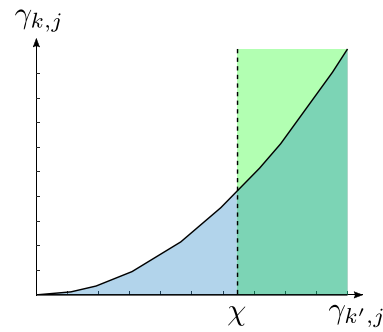


FIGURE 5. Illustration of signal-based inhibited region with threshold χ in green and rate-based inhibited region in blue, in terms of SNR of associated TX $\gamma_{k,j}$ and interfering TX $\gamma_{k',j}$.

We position RXj, located in the association region of TXk, at the boundary with the association region of TXk'. Then $h_{k,j}/h_{k',j} = \epsilon$ with $\epsilon \geq 1$ and $\epsilon \approx 1$ and (16) becomes:

$$\frac{\alpha^2 h_{k,j}^2}{(\alpha^2 h_{k',j}^2)^2} \frac{N}{\Gamma} < 1 \Leftrightarrow \frac{\alpha^2 h_{k,j}^2}{N} > \frac{\epsilon^2}{\Gamma}. \quad (18)$$

This means that, if the SNR ($\alpha^2 h_{k,j}^2/N$) in the association region is large (SNR $> \epsilon^2/\Gamma$), then the inequality holds and as such the inhibited region extends beyond the association region.

Further, (16) can also be expressed in terms of RXj's SNR from the associated TXk $\gamma_{k,j}$, and the interfering TXk' $\gamma_{k',j}$:

$$\frac{\alpha^2 h_{k,j}^2}{(\alpha^2 h_{k',j}^2)^2} \frac{N}{\Gamma} < 1 \Leftrightarrow \gamma_{k,j} < \Gamma \gamma_{k',j}^2. \quad (19)$$

Thus, the contour of the exclusive region is characterized by a quadratic relationship between the SNR of the associated TXk and interfering TXk', as illustrated in Fig. 5. In the figure, also the fixed signal-based inhibited region is depicted. It is clear that the signal-based region only depends on the signal strength of the interfering TXk', while the rate-based region inhibits only transmissions that would create harmful interference above a threshold.

D. VISUALIZATION OF INHIBITED REGIONS

In this section, we visualize the exclusive regions and inhibited regions derived in the previous section. We use identical simulation parameters as in the performance evaluation in Section V. We consider a setup grid of nine TXs with inter-TX distance $\Delta_t = 2.0$ m, as illustrated in Fig. 6. The TX emission pattern is modeled by a Lambertian emission pattern with $\phi_{1/2} = 25^\circ$.

We first focus on the rate-based exclusive region. In Fig. 7, the association region of TX5 is depicted. On top of that, the exclusive regions of TX5 with respect to TX6 $\mathcal{E}_{5,6}^r$ (right to TX5), to TX8 $\mathcal{E}_{5,8}^o$ (up to TX5) and to TX9 $\mathcal{E}_{5,9}^r$ (diagonal to TX5) are visualized. The exclusive regions of the other neighbouring TXs are symmetrical to these and therefore are not shown. We observe that the exclusive regions can be approximated by straight lines, which are visualized for all

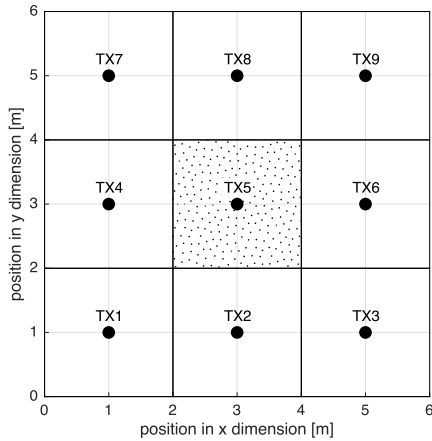


FIGURE 6. Outline of setup consisting of 9 TXs. The association region of TX5 is denoted by the dotted area.

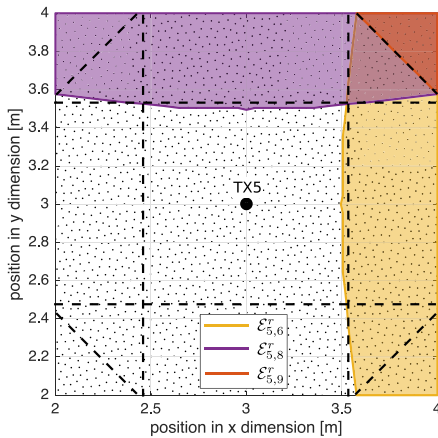


FIGURE 7. Sketch of association region of TX5 denoted in dots, with on top the exclusive regions of TX5 with respect to TX6, TX8 and TX9. These regions can be approximated by straight lines, which are shown by the dashed lines for all eight neighbouring TXs.

eight neighbouring TXs in the figure. By combining these exclusive regions, we observe that the *inhibited* region has an octagonal shape for a rectangular TX deployment, which is shown in Fig. 8 in blue. However, the rate-based inhibited region only has an octagonal shape for a regular rectangular TX grid with exactly eight neighbours. In general, it is a Voronoi polygon defined by (16).

We compare it with the signal-based inhibited region for three different values of χ in Fig. 8. We observe that $\chi = 4$ matches with the rate-based region in the corner, but overestimates some harmful interfering users at the side of the rate-based exclusive region. Using $\chi = 110$ leads to an empty inhibited region, as the size of the inhibited region does not extend beyond its association region. A more detailed comparison between the performance using different χ values is presented in Section V-B.

Our analysis up to here indicates that it is an oversimplification if we consider the inhibited region of TX k' to be purely defined as the region where this TX produces a signal strength that is above a certain threshold power level χ . The latter would give signal-based inhibited regions and the

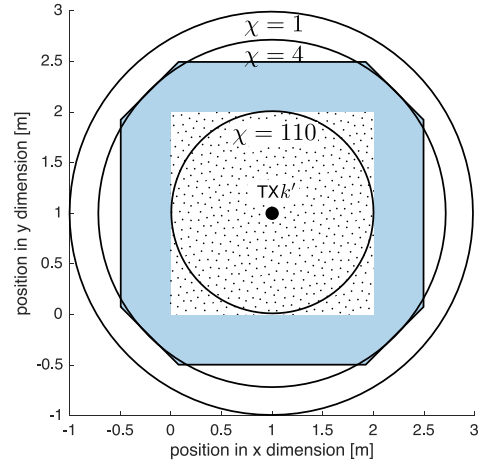


FIGURE 8. Visualization of association region in dots, rate-based inhibited region in blue and contours of the signal-based inhibited region of TX k' in black lines, for $\chi = [1, 4, 110]$.

performance of the scheme depends largely on the threshold. Our rate-based inhibited region instead, is also defined by the signal quality of the TXs which are harmed by this TX k' , which is a ratio of powers and hence does not depend on a threshold that needs to be calibrated.

E. VERIFICATION OF RATE-BASED INHIBITED REGION

In the previous analysis, we focused on the strongest interfering TX and thus neglected the interference from other TXs. In this section, we investigate whether this approximation is reasonable or that a more refined model is needed. To this end, we take into account the interference of all neighbouring TXs.

We do not necessarily restrict our discussion to a rectangular grid and Lambertian emission patterns. In fact, we only rely on the looser assumption that the system is designed in such a way that in the association region of TX k , only the single-hop neighbouring TXs can have significant interference to the associated RXs of TX k . In a rectangular TX deployment as shown in Fig. 6, this means that there are eight possible interfering TXs around the association region of TX k . Therefore, studying a network with nine TXs is sufficient. This also means that maximally $N_c = 4$ time-channels are required, as the top and bottom, or left and right TX, or corner TX can always use the same time-channel by design as they are more than a single-hop away. The set of the TXs which are guaranteed to transmit in the i th time-channel is denoted as $\mathcal{N}_{t,i}$, with $i = 1, \dots, N_c$. For the example in Fig. 6, this gives: $\mathcal{N}_1 = \{5\}$, $\mathcal{N}_2 = \{4, 6\}$, $\mathcal{N}_3 = \{2, 8\}$, $\mathcal{N}_4 = \{1, 3, 7, 9\}$, which also gives a recipe for further spatial extension. However, $N_c = 4$ is a worst-case upper bound, assuming that all exclusive regions have users to be served which is only the case in very dense scenarios. In this section, we are however not optimizing the number of channels, but the shape of the channels. How to find the minimal number of required time-channels will be discussed in Section IV.

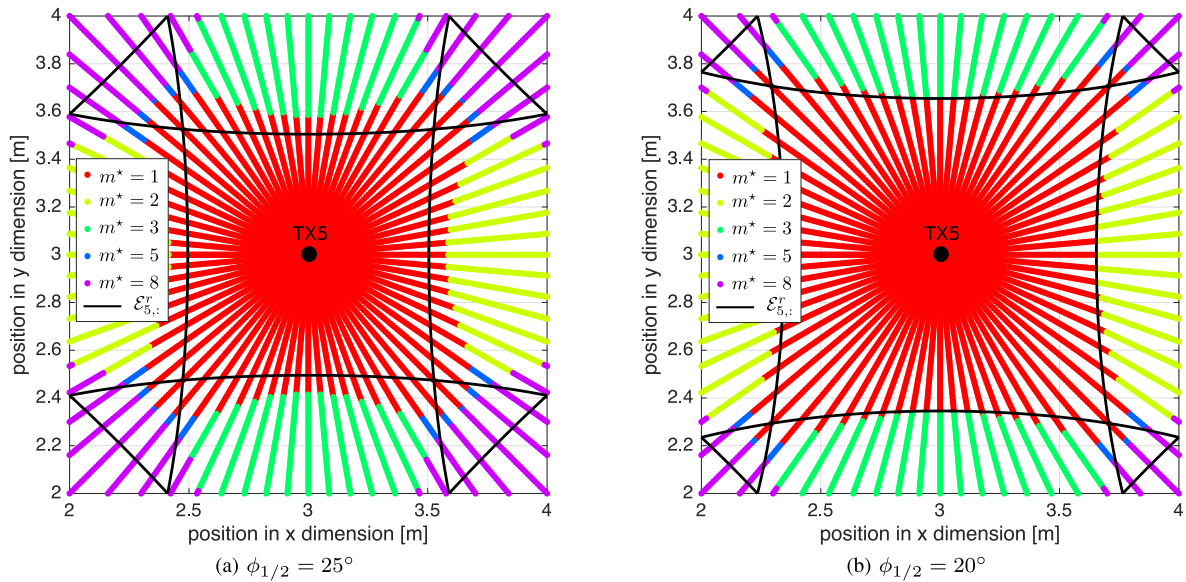


FIGURE 9. Sketch of the association region of TX5. On top of that, the optimal configurations $m^* = \arg \max_m R_m$ are shown in color. The red region denotes the non-exclusive region, the other colors jointly represent the exclusive region. The black lines represent the contours of the rate-based exclusive regions.

TABLE 1. Configurations used in the exhaustive search.

Configuration m	\mathcal{C}_m	$ \mathcal{C}_m $
1	$\{\emptyset\}$	0
2	$\{2\}$	1
3	$\{3\}$	1
4	$\{4\}$	1
5	$\{2, 3\}$	2
6	$\{2, 4\}$	2
7	$\{3, 4\}$	2
8	$\{2, 3, 4\}$	3

The goal is to find the rate-optimal contours for the exclusive region of TX1 with respect to its neighbouring TXs (that can be active at the same time aggregating interference) by performing a brute-force search among all possible active configurations, denoted as index m . Instead of inhibiting TXs, we now inhibit time-channels, as every TX is assigned to one time-channel and the exhaustive search complexity is significantly reduced by doing so. Let us denote \mathcal{C}_m as the set of inhibited time-channels in configuration m . Then, the set of inhibited TXs in configuration m is given by $\mathcal{M}_m = \bigcup_{i \in \mathcal{C}_m} \mathcal{N}_i$. Further, let us denote \mathcal{N}_{all} as the set of all neighbouring TXs, i.e., $\mathcal{N}_{all} = \mathcal{N}_2 \cup \mathcal{N}_3 \cup \mathcal{N}_4$. Assuming RX1 is in the association region of TX5, the data rate of RX1 in configuration $m = [1, \dots, 8]$ can be expressed as:

$$R_m = \frac{B}{1 + |\mathcal{C}_m|} \log_2 \left(\frac{1}{\Gamma} \frac{(\alpha h_{5,1})^2}{N + \lambda} + 1 \right)$$

$$\text{with } \lambda = \sum_{k' \in \{\mathcal{N}_{all} \setminus \mathcal{M}_m\}} (\alpha h_{k',1})^2 \quad (20)$$

in which $|\mathcal{C}_m|$ represents the number of inhibited time-channels. Let us consider $m = 2$ as an example. In this configuration, time-channel 2 is inhibited, meaning that TX4 and TX6 in \mathcal{N}_2 are inhibited to transmit in time-channel 1

when RX1 is active. As time is then shared among these two time-channels, rate is halved, and therefore the throughput to RX1 is divided by $1 + |\mathcal{C}_2| = 2$. In total, there are eight possible configurations, which are listed in Table 1.

By exhaustive search, the optimal configuration $m^* = \arg \max_m R_m$ is determined for many positions of RX1 in the association region of TX5. The result is presented for $\phi_{1/2} = 25^\circ$ and for $\phi_{1/2} = 20^\circ$ in Fig. 9a and Fig. 9b, respectively. We observe that configurations 4, 6 and 7 are never selected, as expected.

The red region (configuration 1) represents the non-exclusive region of TX5 in which none of the neighbouring TXs should be inhibited. For $\phi_{1/2} = 25^\circ$, we conclude that the rate-optimal red region shows a good fit with the rate-based non-exclusive region approximation for a single interferer, which is represented by the inner square formed by the black lines. However, this fit is better for $\phi_{1/2} = 20^\circ$. The reason is that considering only TX5's strongest interfering TX (as the rate-based region does) is more valid if the interference from the other TXs is less pronounced, which is the case if the TX semi-angle $\phi_{1/2}$ is smaller.

We conclude that an approach that only considers the strongest interfering TX in the expression of the exclusive region is reasonable, even for Lambertian emitters that do not exhibit a sharp out-off outside the coverage region.

IV. SPATIALLY EXTENDED TDMA SCHEDULING

Our scheduling algorithm works with a contention-free channel access scheme based on time division multiple access (TDMA). Since it exploits the spatial user distribution to allow or inhibit simultaneous transmissions, we refer to it as Spatially Extended TDMA (SE-TDMA). It is a semi-distributed approach with a two-level architecture consisting of 1) a coarse-grained time-channel scheduler and a

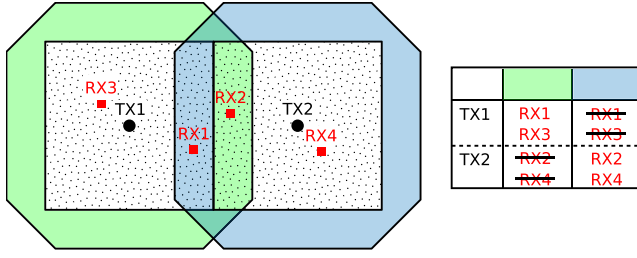


FIGURE 10. Illustration of the time-channel allocation of Algorithm 1, considering the rate-based inhibited region. The association region is denoted by the dotted area. This algorithm is conservative, because the presence of RX1 results in disabling transmissions to all RXs of TX2 in the green time-channel, including RX4, which is a non-exclusive user. However, RX4 could be perfectly served in the green time-channel when TX1 serves one of its non-exclusive users, e.g., RX3.

2) fine-grained time-slot scheduler. The coarse-grained time-channel scheduler is the central aspect of the protocol. Based on the defined inhibited regions, the central controller comes up with a set of time-channels and allocates these to the TXs conservatively, as shown next. Further, it specifies which RX can be served in which time-channel in a distributed way while avoiding harmful interference. This information is then forwarded to the TXs, which use the information from the central controller to implement the fine-grained time scheduler. In their assigned time-channels, the TXs divide the time into smaller scaled time-slots and determine which RX to serve in which time-slot such that the minimal user throughput is maximized. We consider both homogeneous and heterogeneous traffic load conditions across cells. Further, we assume a homogeneous traffic load across users and thus bursty traffic or different (and time-varying) traffic loads per user are not considered. All TXs are assumed to transmit at the same power level, i.e., no power allocation or water filling is performed among the TXs. Both parts will be investigated in more detail below.

A. CENTRALIZED TIME-CHANNEL ALLOCATION

First, the central controller collects the channel information from all nodes in the network and constructs the channel matrix $\mathbf{H} = [h_{k,j}] \in \mathbb{R}^{N_t \times N_r}$, with N_t and N_r the number of TXs and RXs, respectively. Based on this, the protocol determines the association matrix $\mathbf{A} = [a_{k,j}] \in \{0, 1\}^{N_t \times N_r}$, in which $a_{k,j}$ indicates whether RX j is associated to TX k , i.e., $a_{k,j} = 1 \Leftrightarrow j \in \mathcal{A}_k$. To allocate the time-channels among the transmitters, the protocol relies on the inhibited region to know how to avoid harmful interference. To this end, the inhibited matrix $\mathbf{V} = [v_{k',j}] \in \{0, 1\}^{N_t \times N_r}$ is constructed based on the channel matrix, in which $v_{k',j}$ indicates whether RX j is in the inhibited region of TX k' , i.e., $v_{k',j} = 1 \Leftrightarrow j \in \mathcal{I}_{k'}$. The protocol has two options: 1) use the signal-based inhibited region $\mathcal{I}_{k'} = \mathcal{I}_{k'}^s$ with predefined threshold χ or 2) use the rate-based inhibited region $\mathcal{I}_{k'} = \mathcal{I}_{k'}^r$.

Based on the association and inhibited matrix, the minimal number of required time-channels N_c is determined by a recursive algorithm based on the backtracking technique [18]. This recursive algorithm incrementally assigns a time-channel (from 1 to N_c) to each transmitter, while

Algorithm 1: Centralized Time-Channel Allocation

Input : Association matrix $\mathbf{A} \in \{0, 1\}^{N_t \times N_r}$,
inhibited matrix $\mathbf{V} \in \{0, 1\}^{N_t \times N_r}$,
time-channel vector $\boldsymbol{\tau} \in \mathbb{R}^{N_t \times 1}$

Output: Binary time-channel allocation tensor
 $\mathbf{T} \in \{0, 1\}^{N_t \times N_r \times N_c}$

```

1 for  $k = 1$  to  $N_t$  do
2    $\mathcal{A} = \{j \in \mathcal{N}_r \mid a_{k,j} = 1\}$ ;
3   for  $j \in \mathcal{A}$  do
4     if  $\sum_{k'=1}^{N_t} v_{k',j} = 0$  then
5        $t_{k,j,i} = 1, i = [1, \dots, N_c]$ ;
6     end
7   end
8 end
9 for  $k = 1$  to  $N_t$  do
10   $\mathcal{A} = \{j \in \mathcal{N}_r \mid a_{k,j} = 1\}$ ;
11  for  $j \in \mathcal{A}$  do
12    if  $\sum_{k'=1}^{N_t} v_{k',j} > 0$  then
13       $\mathcal{B} = \{k' \in \mathcal{N}_t \mid v_{k',j} = 1, k' \neq k\}$ ;
14       $t_{k,j,\tau_k} = 1$ ;
15       $t_{k',j',\tau_k} = 0, k' \in \mathcal{B}, \forall j' \in \mathcal{N}_r$ ;
16    end
17  end
18 end

```

removing those assignments that fail to satisfy the following constraint: two transmitters TX k and TX k' should not be assigned the same time-channel if there exists a RX j which is both in the association region of TX k and in the inhibited region of TX k' . The algorithm starts with a single time-channel $N_c = 1$ and tries to find a solution. If a solution is not found, then N_c is incremented and the process is repeated, until maximally $N_c = 4$ time-channels.² For example, in Fig. 10, one time-channel is not enough, due to the presence of exclusive users RX1 and RX2. Therefore, $N_c = 2$ time-channels are required for this setup. As a result of the backtracking algorithm, every TX k is assigned a single time-channel, which is represented by τ_k . Together, they form the time-channel vector $\boldsymbol{\tau} = [\tau_k] \in \mathbb{R}^{N_t \times 1}$ with $\tau_k \in [1, \dots, N_c]$. In this time-channel τ_k , TX k is guaranteed to transmit. However, TX k might also transmit in another time-channel $i \neq \tau_k$, as shown next.

Once these matrices are determined, the time-channel allocation tensor $\mathbf{T} = [t_{k,j,i}] \in \{0, 1\}^{N_t \times N_r \times N_c}$ can be constructed, in which $t_{k,j,i}$ indicates whether TX k is allowed to transmit to RX j in time-channel i . The algorithm is presented in Algorithm 1 and works as follows. First, in line 1-8, all N_c time-channels are assigned to the non-exclusive RXs. Then, for the exclusive RXs, in line 9-18, the following rule

2. Maximally $N_c = 4$ time-channels are required, as a RX associated to TX k can maximally be located in the inhibited region of 3 neighbouring TX k' (assuming only significant interference from single-hop neighbours). In that case, 4 time-channels are needed to make sure none of these 4 TXs (including TX k) are active simultaneously.

Algorithm 2: Distributed Time-Slot Scheduling

Input : Time-Channel allocation tensor
 $\mathbf{T} \in \{0, 1\}^{N_t \times N_r \times N_c}$

Output: Time-Slot scheduling tensor
 $\mathbf{F} \in \{0, 1\}^{N_t \times N_r \times N_s}$

```

1  $\bar{\mathbf{R}}_0 = [0] \in \mathbb{R}^{N_r \times 1}$ ;
2 for  $s = 1$  to  $N_s$  do
3   for  $k = 1$  to  $N_t$  do
4      $\mathcal{D} = \{j \in \mathcal{N}_r \mid t_{k,j,v(s)} = 1\}$ ;
5      $j^* = \arg \min_{j \in \mathcal{D}} \bar{R}_{s,j}$ ;
6      $f_{k,j^*,s} = 1$ ;
7   end
8   If applicable, run opportunistic scheduling add-on
   in Algorithm ;
9    $\bar{\mathbf{R}}_s = \bar{\mathbf{R}}_{s-1} + B \log_2(\text{SINR}(\mathbf{F}) + 1)$ ;
10 end

```

is applied. If a TX k has an RX j which is located in the inhibited region of a neighbouring TX k' :

- 1) TX k restricts the RX j to its allocated time-channel τ_k ;
- 2) the neighbouring TX k' restricts all its associated RXs by excluding them from this time-channel τ_k .

Thus, TX k is guaranteed to send in time-channel τ_k to its exclusive users. However, TX k can also transmit to its non-exclusive users in the time-channel of TX k' as long as there is not any RX associated to TX k' located in the inhibited region of TX k .

The controller schedules the users conservatively, as all transmissions by TX k' are disabled in time-channel τ_k when there is at least one RX j associated to TX k that is in the inhibited region of TX k' . However, not all RX $j' \neq j$ associated with TX k might be harmed by TX k' , e.g., RX3 in Fig. 10 is not harmed by TX2. As a result, slots are wasted when TX1 locally schedules RX3, as TX2 is silenced although it could also serve RX4 without causing harmful interference. Below, we discuss the local distributed scheduling algorithm, and also explain how neighbours can coordinate to opportunistically schedule non-exclusive users such that no slots are wasted.

B. DISTRIBUTED TIME-SLOT SCHEDULING

Once the time-channel allocation tensor \mathbf{T} is constructed, every TX k receives its part $t_{k,j,i}$, $\forall j \in \mathcal{N}_r$, $i = [1, \dots, N_c]$, specifying which RX j the TX k is allowed to serve in time-channel i . Based on this information, every TX k schedules its RXs in a local and distributed way in time over the N_s considered time-slots. During these N_s time-slots, the channel matrix is assumed to be static. In this work, we consider a scheduler that aims to maximize the minimal user throughput. To accomplish this, every TX keeps track of the cumulative RX throughput $\bar{\mathbf{R}}_s = [\bar{R}_{s,j}] \in \mathbb{R}^{N_r \times 1}$ up to the current time-slot s , which is given by $\bar{R}_{s,j} = \sum_{s'=1}^s R_{s',j}$ with $R_{s',j}$ the throughput to RX j in time-slot s' . In every time-slot the TX is allowed to transmit, it selects the RX in

Algorithm 3: Opportunistic Scheduling Add-On

```

1 for  $k' = 1$  to  $N_t$  do
2    $\mathcal{D} = \{j \in \mathcal{N}_r \mid t_{k',j,v(s)} = 1\}$ ;
3   if  $\mathcal{D} = \emptyset \wedge (\nexists j, \nexists k: v_{k',j} = 1 \wedge f_{k,j,s} = 1)$  then
4      $\mathcal{F} = \{j \in \mathcal{N}_r \mid a_{k',j} = 1 \wedge \sum_{k=1}^{N_t} v_{k,j} = 0\}$ ;
5      $j^* = \arg \min_{j \in \mathcal{F}} R_{s,j}$ ;
6      $f_{k',j^*,s} = 1$ ;
7   end
8 end

```

its association region with the least throughput so far. The algorithm is presented in Algorithm 2. The time-slots are divided over the time-channels proportional to the average user density per cell in each time-channel. For example, for a homogeneous traffic load across the cells, the time-slots are equally divided over the time-channels. The resulting active time-channel in time-slot s is denoted by $v(s)$.

In addition to local scheduling, we propose to use neighbour coordination to fill unused transmission opportunities for non-exclusive users, as outlined in Algorithm 3. First, TX k' verifies that it has no planned transmissions in time-slot s . If this is the case and if there is not any RX j being served by an associated neighbouring TX k which is located in the inhibited region of TX k' , then this TX k' is allowed to transmit in the current time-slot and TX k' selects the RX j' in its non-exclusive region, if any, with the minimal throughput so far.

In this way, unused spots are filled without harming the existing planned transmissions. This comes at the cost of the requirement to exchange fine-grained scheduling information among the TX neighbours, as neighbouring TXs need to notify each other which RX will be served in the next time-slot. We refer to the SE-TDMA algorithm presented before with inclusion of this add-on as Opportunistic SE-TDMA (OSE-TDMA).

C. COMPUTATIONAL COMPLEXITY

The centralized time-channel allocation starts with constructing the association matrix, for which the maximum of a vector of length N_t needs to be found for all N_r users. This gives a computational complexity proportional to $O(N_t N_r)$. The complexity of constructing the inhibited matrix is also $O(N_t N_r)$. The recursive backtracking algorithm has a worst-case computational complexity of $O(N_c^{N_t})$, with maximally $N_c = 4$. To avoid this exponential dependency in terms of N_t , static time-channel allocation can be used instead (in which four fixed time-channels are assigned at installation time based on the spatial TX layout), leading to similar performance as shown next in Section V-D. The complexity of Algorithm 1 is proportional to $O(N_t N_r)$, as for every TX (outer loop), maximally N_r assignments take place (inner loop). Thus, in case the backtracking algorithm is avoided, the complexity of the centralized time-channel allocation scales linearly with number of transmitters N_t and number of receivers N_r .

TABLE 2. System parameters for simulations.

Parameter	Notation	Value
General		
Noise power	N	5.7×10^{-18} W
Communication bandwidth	B	50 MHz
Implementation gap	Γ	4
Transmitter		
Half power semi-angle	$\phi_{1/2}$	25°
Transmission power	P_c	1.3 W
Wall-plug efficiency	η	0.40
Receiver		
Field-of-view, collection area	Ψ_c, A_{pd}	$60^\circ, 1.1 \text{ mm}^2$
Responsivity	ρ	0.40 A/W

The time-slot scheduling functionality is distributed over the transmitters. In each time-slot, Algorithm 2 finds the minimum of a vector consisting of maximally N_r elements, which has a complexity of $O(N_r)$. Also complexity of the opportunistic scheduling add-on in Algorithm 3 is $O(N_r)$ for each TX. For all TXs together, this gives a complexity of $O(N_t N_r)$. Thus, we conclude that the complexity of the distributed time-slot scheduling also scales linearly with N_t and N_r . Although the computational complexity is similar for the centralized and distributed approach, the latter requires a higher communication overhead since information needs to be transferred from the central controller to the TXs as well as between the TXs.

V. PERFORMANCE EVALUATION

In this section, we simulate the scheduling protocols presented in Section IV, considering both the signal-based and rate-based inhibited region discussed in Section III. The protocols do not require knowledge of the RX positions, and are exclusively based on the channel qualities. The simulation setup considered in the performance evaluation is described below. A selection of relevant system parameters is presented in Table 2.

A. SIMULATION SETUP

We consider a large-scale LiFi network with $N_t = 16$ TXs. Every TX is positioned at a height of 2.8 m and has a Lambertian emission pattern with a semi-angle $\phi_{1/2} = 25^\circ$, unless specified otherwise. Inspired by the specifications of the Luxeon Rebel LXMLPB02-0023 LED which has a flat frequency response up to 50 MHz [17], we consider a communication bandwidth $B = 50$ MHz.

The N_r RXs are uniformly distributed in the network with a minimal inter-RX distance of 25 cm and height of 0.8 m. The field-of-view of the RX is $\Psi_c = 60^\circ$. By default, we assume that every cell has the same number of active RXs $N_{r,cell}$, resulting in a total number of RXs $N_r = N_t \times N_{r,cell}$. We vary the number of RXs per cell from $N_{r,cell} = 1$ to $N_{r,cell} = 8$. However, we also study heterogeneous traffic load across cells in Section V-D. The fairness among the users is analyzed according to the Jain Fairness Index.

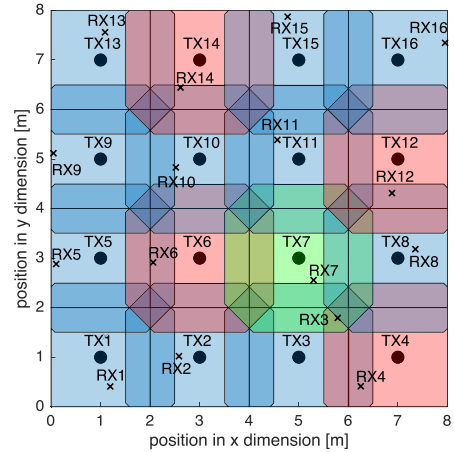


FIGURE 11. Snapshot of a particular network layout with $N_{r,cell} = 1$. The rate-based in inhibited region is visualized for all $N_t = 16$ TXs. The color of the regions represent the assigned time-channel τ_k of TX k . For this distribution, $N_c = 3$ time-channels are sufficient.

Each MAC cycle has a duration of $T_{mac} = 40$ ms and is divided in $N_{s,mac} = 16$ time-slots. The time-slots are distributed over the time-channels proportional to the average user density per cell in each time-channel. For example, for homogeneous traffic load across the cells, the time-slots are equally distributed over the time-channels. Thus, if four time-channels are used, every time-channel will be active for four time-slots within a MAC cycle.

We assume that the channel matrix is static during every $N_{mac} = 25$ MAC cycles, corresponding to $N_s = N_{s,mac} \times N_{mac} = 400$ time-slots. After this time, the RXs change their location. In total, 50 different random RX layouts are considered.

A snapshot of an exemplary network layout with a single RX per cell, considering the rate-based inhibited region is depicted in Fig. 11. For this RX distribution, the recursive algorithm obtains a feasible time-channel allocation using $N_c = 3$, so three time-channels are sufficient. The assigned time-channels τ_k to the TXs are denoted in blue, red and green in the figure.

Although we focus on stationary users in the evaluation, we emphasize that the protocol can also cope with mobile users, as long as the channel is measured frequently enough. That is, the protocol has a low complexity and hence can provide the time-slot schedule based on the CSI in a timely manner, facilitating mobile users.

B. IMPACT OF SIGNAL-BASED INHIBITED REGION SIZE

We compare the performance of SE-TDMA using the rate-based inhibited region with three different signal-based inhibited regions, which were visualized before in Fig. 8:

- 1) Extremely small signal-based inhibited region $\mathcal{I}_{k'}^s$ ($\chi = 110$, corresponding to SNR threshold of 20.4 dB): the SNR threshold is so large that the inhibited region is empty, which means that parallel transmissions are never prohibited and thus are always tolerated.

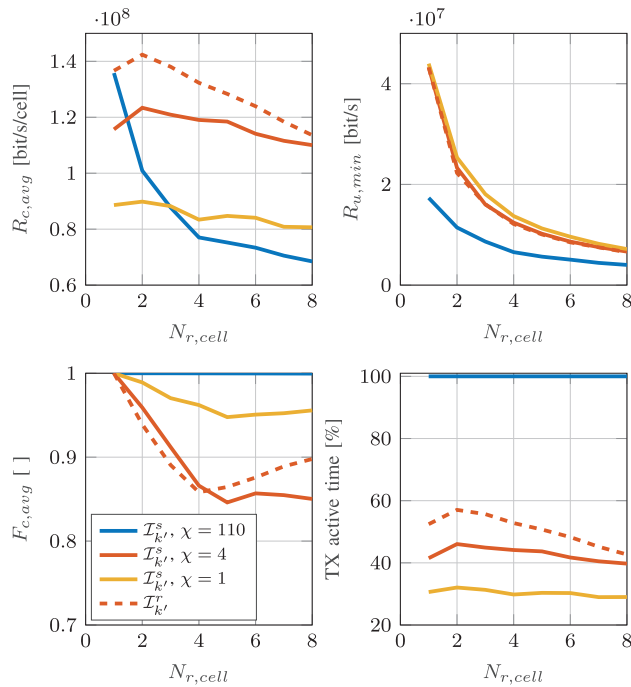


FIGURE 12. Comparison of SE-TDMA considering the rate-based inhibited region $\mathcal{I}_{k'}^r$ and the signal-based inhibited region $\mathcal{I}_{k'}^s$ with different thresholds χ , in terms of average cell throughput $R_{c,avg}$ (top left), minimal user throughput $R_{u,min}$ (top right), average cell user fairness $F_{c,avg}$ (bottom left) and TX active time (bottom right).

- 2) Extremely large signal-based inhibited region $\mathcal{I}_{k'}^s$ ($\chi = 1$, corresponding to SNR threshold of 0 dB): the SNR threshold is very small such that as soon as a RX can decode information of a particular TXk (i.e., in the coverage region of TXk), it is also considered to be in the inhibited region of TXk. This results in a large inhibited region and thus the algorithm is very conservative in allowing parallel transmissions.
- 3) Matching signal-based inhibited region $\mathcal{I}_{k'}^s$ ($\chi = 4$, corresponding to SNR threshold of 6.0 dB): the SNR threshold is set such that it matches with the rate-based inhibited region in the corners of the octagonal region (assuming all RXs are facing upwards, and all RXs have the same field-of-view). This should lead to a similar performance as the rate-based inhibited region.

The resulting performance is shown in Fig. 12. We focus first on the signal-based inhibited region. We observe that considering the empty inhibited region ($\chi = 110$), the TX active time is 100% (fraction of time-slots that the TX is actually transmitting information to its associated RXs), thus all transmitters are always active. This comes at the cost of significant harmful interference among the users, which results in a low cell throughput and low minimal user throughput. By using a very conservative inhibited region instead ($\chi = 1$), the interference can be reduced but the transmitters can only transmit in 30% of the time on average. Therefore, the cell throughput is still limited. The minimal user throughput is increased because when a transmitter is active, it can send

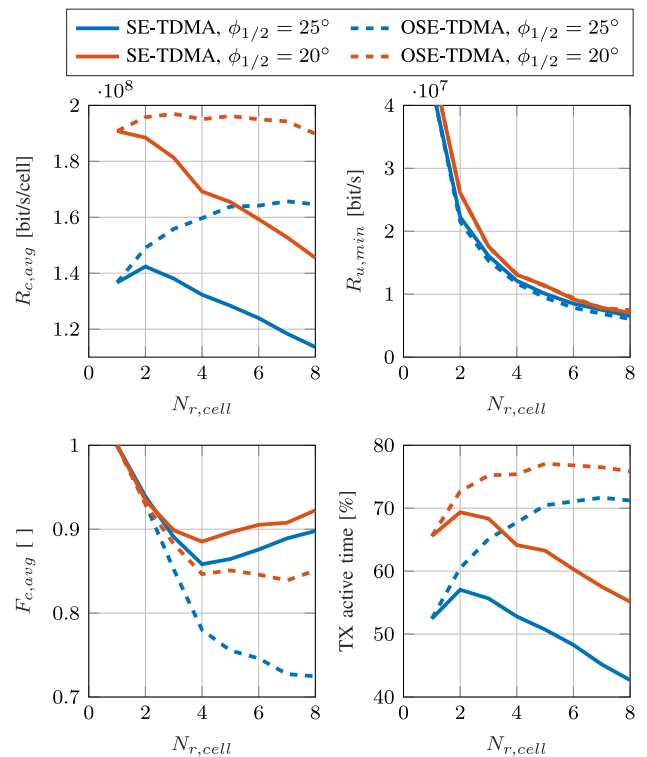


FIGURE 13. Comparison of SE-TDMA and OSE-TDMA considering the rate-based inhibited region, in terms of average cell throughput $R_{c,avg}$ (top left), minimal user throughput $R_{u,min}$ (top right), average cell user fairness $F_{c,avg}$ (bottom left) and TX active time (bottom right). Both the result for $\phi_{1/2} = 25^\circ$ and $\phi_{1/2} = 20^\circ$ is shown.

with almost no interference. Using $\chi = 4$ strikes a good balance between the two aforementioned extreme choices of χ . The rate-based inhibited region shows the highest cell throughput. As expected from Fig. 8, the TX active time using the rate-based inhibited region is slightly larger than $\chi = 4$, because the rate-based inhibited region is slightly smaller in area size and thus is less conservative in prohibiting transmissions. Compared to $\chi = 1$, the rate-based region improves the cell throughput with 41% for $N_{r,cell} = 8$, while realizing a very similar minimal user throughput.

We conclude that the rate-based inhibited region is the preferred choice for the inhibited region, as it fully adapts to the environment, i.e., it works for different RX orientations and different RX heights. This is in contrast with the signal-based inhibited region, which depends on a fixed threshold χ that needs to be adapted at run-time to the conditions of the environment to be able to keep matching with the rate-based region.

C. IMPACT OF OPPORTUNISTIC SCHEDULING

We analyze the impact of opportunistic scheduling, given in Algorithm 3, on the system performance. We refer to the baseline SE-TDMA algorithm with inclusion of this add-on as Opportunistic SE-TDMA (OSE-TDMA). We consider the rate-based inhibited region and compare algorithms SE-TDMA and OSE-TDMA for both a setup with $\phi_{1/2} = 25^\circ$ and $\phi_{1/2} = 20^\circ$, keeping the TX transmission power constant. The simulation results are shown in Fig. 13.

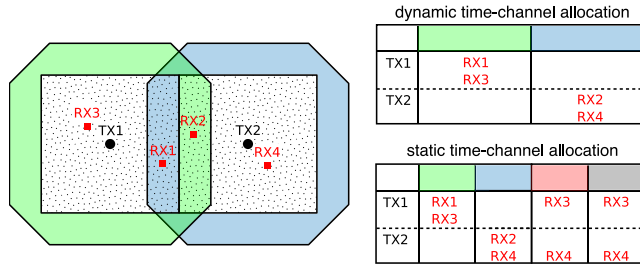


FIGURE 14. Comparison between dynamic and static time-channel allocation in SE-TDMA considering the rate-based inhibited region. The association region is denoted by the dotted area.

We observe that OSE-TDMA results in a higher cell throughput for both TX semi-angles. This is because unused transmission opportunities are filled, and thus a higher TX active time is observed. This results in an increase of 45% and 30% in cell throughput with $N_{r,cell} = 8$ for $\phi_{1/2} = 25^\circ$ and $\phi_{1/2} = 20^\circ$, respectively. We observe that this gain in throughput is realized by boosting the throughput to some users, without significantly reducing the minimal user throughput. As a result, the Jain Fairness Index is lower. Next, we note that the cell throughput for OSE-TDMA shows a less decreasing trend in terms of user density compared to SE-TDMA, from which we conclude that the former can better cope with dense user deployments.

Further, we conclude that the cell throughput is higher for $\phi_{1/2} = 20^\circ$ compared to $\phi_{1/2} = 25^\circ$. The reason is two-fold: 1) the smaller TX semi-angle, the more confined the transmission power is in the association region of the TXs and the less interference is generated in the association regions of neighbouring TXs and 2) as shown in Fig. 9b, the non-exclusive region for the smaller TX semi-angle is larger, implying that the protocol allows more simultaneous transmissions. The latter is also visible in the higher TX active time for $\phi_{1/2} = 20^\circ$ compared to $\phi_{1/2} = 25^\circ$.

D. FOUR STATIC TIME-CHANNELS

Instead of dynamically determining the minimal number of required N_c time-channels with the backtracking algorithm, we compare its performance with having four static time-channels. We do not consider OSE-TDMA in this paragraph. To emphasize the difference between these two methods, the former and the latter are here referred to as dynamic SE-TDMA and static SE-TDMA, respectively. In static SE-TDMA, the $N_c = 4$ static time-channels are assigned once at installation time to the TXs based on the spatial TX layout. They do not change over time and they are independent of the RX distribution in the network. An example is presented in Fig. 14. As there are only two conflicting transmitters, $N_c = 2$ instead of $N_c = 4$ time-channels are found to be sufficient by the backtracking algorithm in the dynamic allocation, instead of always using four time-channels in the static allocation. The simulation result is shown in Fig. 15. The difference between the dynamic and static time-channel allocation is marginal. Therefore, we

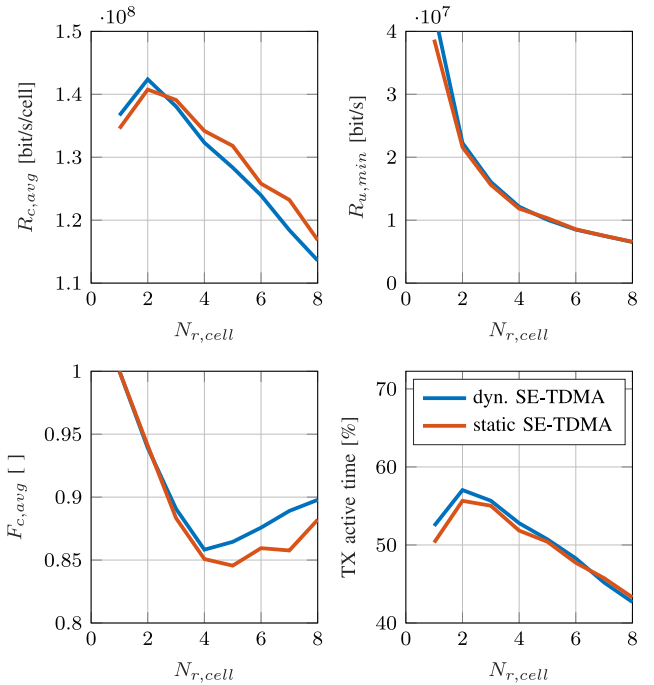


FIGURE 15. Comparison of dynamic SE-TDMA and static SE-TDMA considering the rate-based inhibited region, in terms of average cell throughput $R_{c,avg}$ (top left), minimal user throughput $R_{u,min}$ (top right), average cell user fairness $F_{c,avg}$ (bottom left) and TX active time (bottom right).

conclude that the complexity of the scheduler can be further reduced by avoiding the backtracking algorithm (which takes on average 1.36 s for $N_{r,cell} = 1$ and 33 ms for $N_{r,cell} = 8$). However, by using static time-channels, there still needs to be an initial algorithm to collect the transmitter neighbour relations and construct the inhibited matrix.

E. HETEROGENEOUS TRAFFIC LOAD ACROSS CELLS

We study the impact of a heterogeneous traffic load across cells on the system performance. Instead of placing the users randomly in each cell, we now place the users randomly in the entire environment, resulting in a different number of users in each cell. A comparison between a homogeneous and heterogeneous traffic load is shown in Fig. 16. As expected, we observe a slightly smaller minimal user throughput for the heterogeneous traffic load compared to the homogeneous load, for both SE-TDMA and OSE-TDMA. Further, we notice at low user density a higher cell throughput for the heterogeneous traffic load compared to a homogeneous load. This is because some cells might be unoccupied at low user density, leading to a smaller number of required time-channels and a higher active time for the TXs as there is less interference across cells.

F. COMPARISON WITH RELATED WORK

We compare the performance of SE-TDMA with two related state-of-the-art research works in LiFi scheduling.

1) RX GROUPING

In [12], an interference management algorithm for a cell-free Visible Light Communication (VLC) network is proposed by

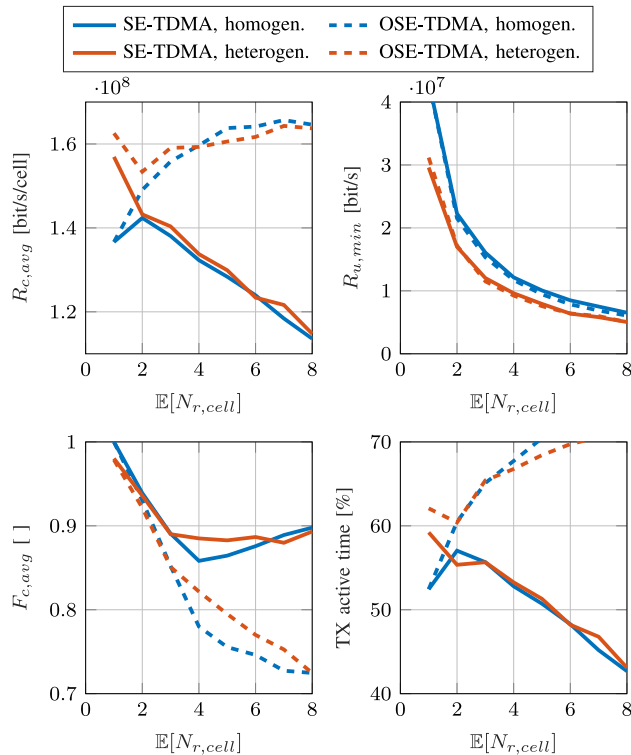


FIGURE 16. Comparison of SE-TDMA and OSE-TDMA considering the rate-based inhibited region, in terms of average cell throughput $R_{c,avg}$ (top left), minimal user throughput $R_{u,min}$ (top right), average cell user fairness $F_{c,avg}$ (bottom left) and TX active time (bottom right). $\mathbb{E}[N_{r,cell}]$ denotes the expected number of users per cell. Both the result for homogeneous and heterogeneous traffic load across cells is shown.

joint design of user scheduling and precoding. The users are divided in user groups, for which the time fractions these user groups will be served are optimized. In every user group, MIMO is performed with precoding based on signal-to-leakage-and-noise ratio (SLNR) instead of zero-forcing. In this way, in contrast to zero-forcing, the number of users can be larger than the number of transmitters.

Due to the large size of feasible user groups (e.g., a network with 15 users already has $|\mathcal{U}| = 32767$ possible user groups), the optimization problem is complex, as it has to find the optimal time fraction vector with $|\mathcal{U}|$ elements. Therefore, similarly as in [12], user groups with a low probability of being selected are removed to reduce the size of \mathcal{U} . Hence, a user group is omitted if there exists a user pair with a inter-user distance smaller than 1.25 m.

2) TX GROUPING

In [8], the authors look at the problem from a different perspective. Instead of focusing on grouping the receivers, here they aim to optimally partition the TXs in different transmitter groups. First, the TX partitioning is performed, based on the constructed interference graph. In a second step, the time fractions are optimized of the RXs which should be served by these TX groups. They consider a SISO architecture, so a single TX communicates with a single RX and precoding is not performed. Further, only TXs within the same TX group can be active simultaneously, so there

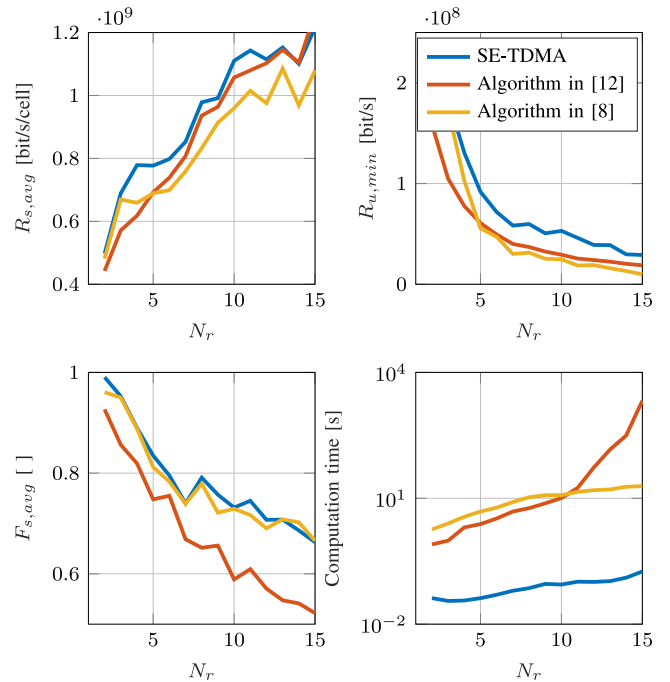


FIGURE 17. Comparison between dynamic SE-TDMA considering the rate-based inhibited region, algorithm in [12] and algorithm in [8], in terms of average cell throughput $R_{c,avg}$ (top left), minimal user throughput $R_{u,min}$ (top right), average cell user fairness $F_{c,avg}$ (bottom left) and average computation time (bottom right) in function of number of RXs N_r .

is no interference among different TX groups. To ensure a fair comparison with our algorithm, we assume that all transmitters use a fixed power and the optimization of power allocation among the transmitters in [8] is not implemented.

Due to the high complexity of the algorithms presented above, a smaller network with only $N_t = 9$ TXs, $N_r = [2, \dots, 15]$ RXs and 25 different RX layouts is considered. Instead of cell-wide metrics, we now consider network-wide metrics because not every cell is occupied if $N_r < N_t$. A comparison of these two related works with SE-TDMA using the rate-based inhibited region is shown in Fig. 17. Averaged over the different user densities N_r , we observe that SE-TDMA shows a slightly larger system throughput of 7% and 12% compared to the algorithm in [12] and [8], respectively. Further, the minimal user throughput of SE-TDMA shows a gain of 60% and 91%, respectively. To get more insight in the throughput distribution, the cumulative distribution function (CDF) of the minimal user throughput and average user throughput in a network with $N_r = 15$ users is depicted in Fig. 18.

Since a complete set of all feasible user groups is considered in [12], the computational complexity is high. This makes it impractical to run on large networks as the resulting network latency will be too large, especially for highly mobile traffic loads (see Fig. 17 bottom right). For example, in a network with $N_r = 15$ users, the average computation time for a single RX layout equals 2119 s for the algorithm in [12] versus only 180 ms for SE-TDMA. Averaged over the different numbers of users N_r , SE-TDMA can reduce the complexity by a factor of 1200. Although the authors

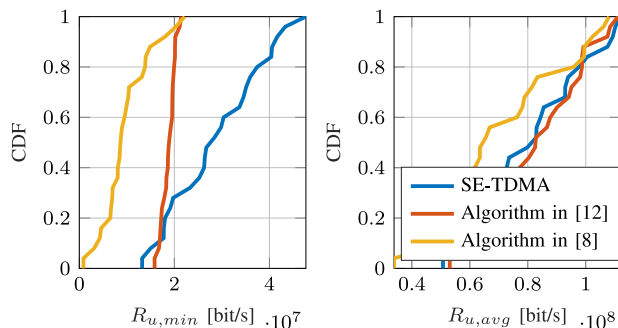


FIGURE 18. CDF of minimal user throughput $R_{u,min}$ (left) and average user throughput $R_{u,avg}$ (right) in a network with $N_r = 15$ users. A comparison is made of SE-TDMA considering the rate-based inhibited region, algorithm in [12] and algorithm in [8].

state that the algorithm in [8] can find a solution with rather low complexity, we notice a significant gain of SE-TDMA in the computation time. For example, in a network with $N_r = 15$ users the computation time for a single RX layout equals 19.5 s for the algorithm in [8]. Averaged over N_r , SE-TDMA can achieve a reduction in complexity by a factor of 120.

VI. CONCLUSION

Motivated by the high complexity of scheduling algorithms for LiFi networks, we propose a semi-distributed Spatially Extended TDMA algorithm that can reduce the computational complexity by at least a factor 120, while improving the minimal user throughput up to 91%, compared to state-of-the-art research in LiFi. To achieve this, we first derived practical and exact expressions to determine which transmissions will create harmful interference. Based on these expressions and insights, we propose a solution that partitions users into a subset of non-exclusive users which do not experience harmful interference, and a subset of exclusive users which are harmed and thus need to be scheduled in multiple time-slots. Two metrics for user partitioning are considered: signal-based and rate-based regions, where the latter is shown to have the advantage of not relying on a design parameter or threshold that depends on the scenario, LED or receiver properties. Moreover, our protocol takes a divide-and-conquer approach to implement this solution in an efficient way, while maintaining flexibility so that idle time-slots are avoided when traffic or user locations are not uniformly spread in time or space. The semi-distributed scheduling combined with the rate-based interference regions, achieves comparable average rate compared to the state of the art, while significantly improving fairness and computational cost. As a result, our approach will enable very dense LiFi networks efficiently.

REFERENCES

- [1] V. Jungnickel *et al.*, "LiFi for industrial wireless applications," in *Proc. Opt. Fiber Commun. Conf. Exhibit. (OFC)*, San Diego, CA, USA, 2020, pp. 1–3.
- [2] C. Chen, S. Videv, D. Tsonev, and H. Haas, "Fractional frequency reuse in DCO-OFDM-based optical attocell networks," *IEEE J. Lightw. Technol.*, vol. 33, no. 19, pp. 3986–4000, Oct. 1, 2015.
- [3] H. Kazemi, M. Safari, and H. Haas, "Spectral efficient cooperative downlink transmission schemes for DCO-OFDM-based optical attocell networks," in *Proc. IEEE 84th Veh. Technol. Conf. (VTC)*, Montreal, QC, Canada, 2016, pp. 1–6.
- [4] M. D. Soltani, X. Wu, M. Safari, and H. Haas, "Access point selection in Li-Fi cellular networks with arbitrary receiver orientation," in *Proc. IEEE 27th Annu. Int. Symp. Pers. Indoor Mobile Radio Commun. (PIMRC)*, Valencia, Spain, 2016, pp. 1–6.
- [5] X. Ling, J. Wang, Z. Ding, C. Zhao, and X. Gao, "Efficient OFDMA for LiFi downlink," *IEEE J. Lightw. Technol.*, vol. 36, no. 10, pp. 1928–1943, May 15, 2018.
- [6] Y. Wang, X. Wu, and H. Haas, "Resource allocation in LiFi OFDMA systems," in *Proc. IEEE Global Commun. Conf. (GLOBECOM)*, Singapore, 2017, pp. 1–6.
- [7] R. Jiang, Q. Wang, H. Haas, and Z. Wang, "Joint user association and power allocation for cell-free visible light communication networks," *IEEE J. Sel. Areas Commun.*, vol. 36, no. 1, pp. 136–148, Jan. 2018.
- [8] J. Chen, Z. Wang, and R. Jiang, "Downlink interference management in cell-free VLC network," *IEEE Trans. Veh. Technol.*, vol. 68, no. 9, pp. 9007–9017, Sep. 2019.
- [9] A. M. Abdelhady, O. Amin, A. Chaaban, B. Shihada, and M. S. Alouini, "Downlink resource allocation for dynamic TDMA-based VLC systems," *IEEE Trans. Wireless Commun.*, vol. 18, no. 1, pp. 108–120, Jan. 2019.
- [10] J. Deng, X. Jin, X. Ma, M. Jin, C. Gong, and Z. Xu, "Graph-based scheduling for cooperative transmission in indoor VLC systems," in *Proc. IEEE Int. Conf. Commun. (ICC) Workshops*, Shanghai, China, 2019, pp. 1–6.
- [11] M. Obeed, A. M. Salhab, S. A. Zummo, and M. S. Alouini, "New algorithms for energy-efficient VLC networks with user-centric cell formation," *IEEE Trans. Green Commun. Netw.*, vol. 3, no. 1, pp. 108–121, Mar. 2019.
- [12] J. Chen and Z. Wang, "Joint design of user scheduling and precoding for interference management in cell-free VLC network," in *Proc. IEEE Global Commun. Conf. (GLOBECOM)*, Waikoloa, HI, USA, 2019, pp. 1–6.
- [13] W. Yuan, J.-P. M. G. Linnartz, and I. G. M. M. Niemegeers, "Adaptive CCA for IEEE 802.15.4 wireless sensor networks to mitigate interference," in *Proc. IEEE Wireless Commun. Netw. Conf. (WCNC)*, Sydney, NSW, Australia, 2010, pp. 1–5.
- [14] H. J. Kim and J.-P. M. G. Linnartz, "Virtual cellular network: A new wireless communications architecture with multiple access ports," in *Proc. IEEE Veh. Technol. Conf. (VTC)*, Stockholm, Sweden, 1994, pp. 1055–1059.
- [15] C. van den Broek and J.-P. M. G. Linnartz, "A simulation study of space and time reservation multiple access," in *Proc. IEEE Int. Symp. Pers. Indoor Mobile Radio Commun. (PIMRC)*, vol. 2. Toronto, ON, Canada, 1995, pp. 527–531.
- [16] L. Thiele, V. Jungnickel, and T. Haustein, "Interference management for future cellular OFDMA systems using coordinated multi-point transmission," *IEICE Trans.*, vol. E93B, pp. 3228–3237, Dec. 2010.
- [17] S. Mardankorani, X. Deng, and J.-P. M. G. Linnartz, "Sub-carrier loading strategies for DCO-OFDM LED communication," *IEEE Trans. Commun.*, vol. 68, no. 2, pp. 1101–1117, Feb. 2020.
- [18] G. Brassard and P. Bratley, *Fundamentals of Algorithmics*. Englewood Cliffs, NJ, USA: Prentice-Hall, 1996.